A Computational Model for Temperature and Sterility Distributions in a Pilot-Scale High-Pressure High-Temperature Process

Kai Knoerzer and Pablo Juliano
Innovative Foods Centre, Food Science Australia, Private Bag 16, Werribee, VIC, Australia
Food Futures Flagship, CSIRO, North Ryde, NSW, Australia

Simon Gladman
Innovative Foods Centre, Food Science Australia, Private Bag 16, Werribee, VIC, Australia

Cornelis Versteeg
Innovative Foods Centre, Food Science Australia, Private Bag 16, Werribee, VIC, Australia
Food Futures Flagship, CSIRO, North Ryde, NSW, Australia

Peter J. Fryer
Centre for Formulation Engineering, Chemical Engineering, University of Birmingham, Edgbaston, Birmingham B15 2TT, U.K.

DOI 10.1002/aic.11301
Published online September 28, 2007 in Wiley InterScience (www.interscience.wiley.com).

High pressure high temperature processing is a candidate food sterilization process in which heat is generated volumetrically within the food as a result of rapid pressurization to 600 MPa or higher. For commercial viability the temperature profile in the process should be as uniform as possible. A model has been developed to predict the flow and temperature fields inside a pilot scale (35 L) vessel during the pressure heating, holding and cooling stages of the process. Simulations on the empty vessel show that thermal conduction causes excessive cooling. The model agrees well with experimental results in which thermocouples are used to measure temperature throughout a metallic composite carrier inserted into the vessel. The model is used to design a Polytetrafluoroethylene (PTFE) carrier which produces thermal uniformity within the carrier. Predicted variations of sterility resulting from a process are produced using the F_0*-value distribution. No significant reduction of spores was seen in the empty vessel, while more than 94.6% of the PTFE carrier volume achieved a reduction greater than* 10^{12}*.* © 2007 American Institute of Chemical Engineers *AIChE J,* 53: 2996–3010, 2007
Keywords: food, mathematical modeling, computational fluid dynamics (CFD)

Introduction

High pressure sterilization of foods

The key to a successful food process is the production of safe and palatable food that is attractive to the consumer. Increasingly the consumer is also seeking health benefits from

Correspondence concerning this article should be addressed to K. Knoerzer at kai.knoerzer@csiro.au.

foods.[1] Thermal processing is still the most used method of reducing microbial load and enhancing shelf-life; the problem is avoiding the over-processing associated with excess heating which lowers product quality. For pasteurization it is necessary only to lower the concentration of viable bacteria, but for sterilization it is necessary to inactivate the spores of *C. botulinum* as well, typically requiring temperatures above 115°C.[2]

Conventional canning produces a safe but low-quality commercially sterile product; the slowness of thermal conduction means that the outside of the can must be significantly overprocessed to ensure that the centre of the can is cooked. High temperature short time (HTST) processing may deliver food of a higher quality than canning, but requires rapid heat transfer to the material. One problem remaining is the time to cool the food down after heating; again, thermal conduction is potentially too slow. Alternative HTST heating methods have thus been sought in which food is heated volumetrically, for example by microwaves,[3] radio frequency,[4] or electrical current.[5] Other 'nonthermal' methods have been proposed for microbial reduction, such as the application of high pressure of up to 600 MPa,[6] or pulsed electric fields of order 10–100 kV/cm;[7] however, neither of these processes inactivates bacterial spores, so cannot produce a sterile product.

One new candidate method for HTST sterilization is high pressure high temperature (HPHT) treatment, an emerging preservation method for the development of shelf-stable low-acid food products. It involves combining pressures of 600–800 MPa, and moderate initial chamber temperatures of 60–90°C. During pressurization, the process temperature increases to a point where spores are inactivated;[8,9] the system is held at temperature for some time and then depressurized to reduce the temperature. For instance, pressurization temperatures in the range of 90–116°C together with pressures of 500–700 MPa have been used to inactivate a number of strains of *C. botulinum* spores.[10,11] Koutchma et al.[12] showed that the HPHT process could be validated by applying concepts traditionally used in conventional thermal processing of low-acid foods for the inactivation of classical surrogates, namely *B. stearothermophilus* and *C. sporogenes* PA 3679, at a pressure range of 600–800 MPa and a process temperature range of 91–108°C. Their results suggest that the traditional *F*-value approach can be used, which relates the process to the equivalent time at some reference temperature T_{ref}, where temperature T varies with time t:

$$F = \int_0^t 10^{\frac{T(t)-T_{ref}}{z_T}}\, dt = D \log_{10} \frac{N}{N_0} \tag{1}$$

where F is the time the material would be held at T_{ref} to achieve the same microbial destruction as the process, z_T is the temperature increment that changes the rate of the process by a factor of 10, N and N_0 are the final and initial number of spores and D the time at T_{ref} to lower the number of spores by a factor of 10.

The temperature reached during pressurization can be readily derived assuming no thermal losses. If the variation in entropy ds in the system is a function of both temperature and pressure, i.e., $s = f[T, P]$, then:

$$ds = \left(\frac{\partial s}{\partial T}\right)_P dT + \left(\frac{\partial s}{\partial P}\right)_T dP \tag{2}$$

If the process is assumed reversible, the total entropy change is zero. Rearranging, compression heating rate can be expressed as:

$$\frac{dT}{dP} = -\frac{\left(\frac{\partial s}{\partial P}\right)_T}{\left(\frac{\partial s}{\partial T}\right)_P} = \frac{V\left(\frac{1}{V}\left(\frac{\partial V}{\partial T}\right)_P\right)}{\frac{1}{T}\left(T\left(\frac{\partial s}{\partial T}\right)_P\right)} = \frac{T\alpha_p}{\rho C_p} \tag{3}$$

using the appropriate Maxwell's relation:

$$\left(\frac{\partial s}{\partial P}\right)_T = -\left(\frac{\partial V}{\partial T}\right)_P \tag{4}$$

expressing the specific volume V (m^3/kg) as the inverse of the density ρ and defining the thermal expansion coefficient α_p and the isobaric heat capacity C_p as:

$$C_P = T\left(\frac{\partial s}{\partial T}\right)_P \quad \alpha_P = \frac{1}{V}\left(\frac{\partial V}{\partial T}\right)_P \tag{5}$$

On decompression, the process reverses and the temperature decreases. This method, with both rapid heating and cooling, offers the potential of producing high-quality shelf-stable product.

In general, compression/decompression curves are nearly linear, as shown in Figure 1. Compression heating of the transmitting fluid and food will be higher at initial temperatures between 75 and 90°C. Near room temperature, water typically changes 3°C/100 MPa, whereas at 80°C compression heating changes 4.4°C/100 MPa.[10,13] Both product and compression fluid temperature may rise 20–40°C during high-pressure treatment, but the metal pressure vessel will not undergo significant compression heating.[13,14] Rates of 3 MPa/s or greater can be obtained using a high pumping speed with an internal intensifier[10,15] or with an external intensifier in commercial systems.[16]

Several pressure-temperature combinations have been proposed for spore inactivation,[15,17,18] among which application of pressures greater than 600 MPa with short holding times

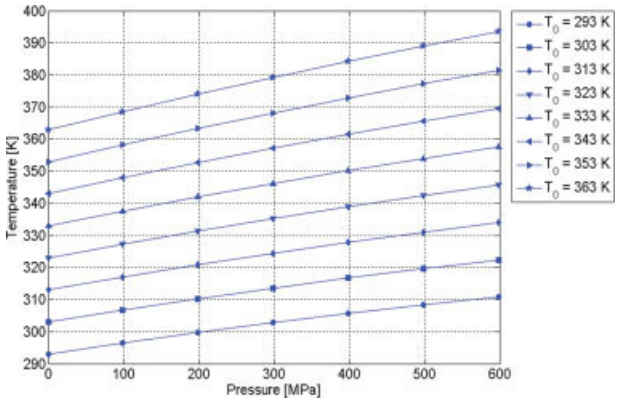

Figure 1. Compression heating curves obtained by integrating Eq. 3 show nearly linear increase of temperature with pressure at selected starting temperatures.

[Color figure can be viewed in the online issue, which is available at www.interscience.wiley.com.]

(5 min or less) seems most economical and safe for industrial purposes. HPHT has demonstrated potential to provide foods with higher pigment, flavor, and nutrient retention among other improved sensory attributes.[8,18–20] To demonstrate the potential of the process to the industry, in addition to demonstrating the quality and consumer acceptability of the product, it is necessary to prove that it can be operated predictably, repeatedly, and safely at pilot scale.

Process models

The design of thermal process operations requires the use of models able to predict the temperature distribution during treatment inside a processing unit. This is necessary both for process design, scale-up, and specification and for governmental regulators to approve the process. The temperature history of a HPHT processed food will be determined by a number of processing steps (i) product preheating and equilibration (ii) pressurization and compression heating (iii) pressure holding and the effect of heat removal through the vessel wall (iv) temperature decrease during decompression, and (v) subsequent cooling. Since compression heating in the steel vessel is almost zero, because of the low compressibility of solids and the low heat release at compression,[13,15] a thermal gradient is developed,[21,22] leading to heat loss towards the chamber wall which becomes a cold region.

Before being able to evaluate the process, the uniformity of the process must be identified, modeled, and validated. Understanding temperature uniformity in a HPHT process is key to prove inactivation of target microorganisms and enzymes. If small amounts of heat are lost throughout the pressure-temperature history of the HPHT process, this may bring significant effects on the inactivation rate of microbial spores.[15,23,24] Thermal gradients established during compression and holding will cause inhomogeneities in the inactivation of target microorganisms and enzymes resulting in over-processed fractions inside the vessel to ensure that the coldest spot is sufficiently heated.[21,22,25-29]

A number of authors have considered thermal effects during high-pressure pasteurization and freezing. Otero and Sanz[22] reviewed literature on thermophysical properties as well as models for heating and freezing under pressurized conditions. Hartmann,[30] Hartmann and Delgado,[31,32] and Hartmann et al.[27] presented a series of models in which convective flows and heat transfer were modeled during pressurization, and also considered the resulting distribution of enzyme and bacteria inactivation resulting from differences in thermal history. More recently, Otero et al.[33] and Ghani and Farid[34] developed models for calculating flow and temperature distributions which occur during high-pressure-low-temperature processing (process temperatures below 60°C and pressures below or equal to 500 MPa). Both showed the resulting temperature effects and found significant temperatures differences throughout the vessel. Otero et al.[33] validated their pasteurization model using thermocouples embedded in agar, and showed differences of up to 10°C between wall and central regions; for an initial temperature of 20°C, final temperatures between 20 and 30°C were seen.

The reactions which lead to inactivation of spores and thus to sterility are highly temperature dependent; common Z_T values for *C. botulinum* are 10°C, implying the rate increases 10-fold for every 10°C rise in temperature.[35] Thermal inhomogeneities must thus be minimized in any sterilization process to ensure uniform processing and maximize the quality of the final product. No work on thermal fluid dynamic modeling of high-pressure-high-temperature sterilization processes has been published to date. The aim of this article was to develop and validate an appropriate mathematical model for the pilot-scale HPHT process currently in operation at Food Science Australia. The model can reproduce the features of the temperature-time profile found in practice in the device, and can calculate the effect of the process on bacterial spores. This type of calculation forms the basis for validation of design calculations for candidate processes.

Materials and Methods

High pressure system

A Flow Pressure Systems QUINTUS® Food Press Type 35L-600 sterilization machine (Avure Technologies, Kent, WA) is one of the few existing pilot systems built for HPHT performance. The system, shown in Figure 2a, consists of a

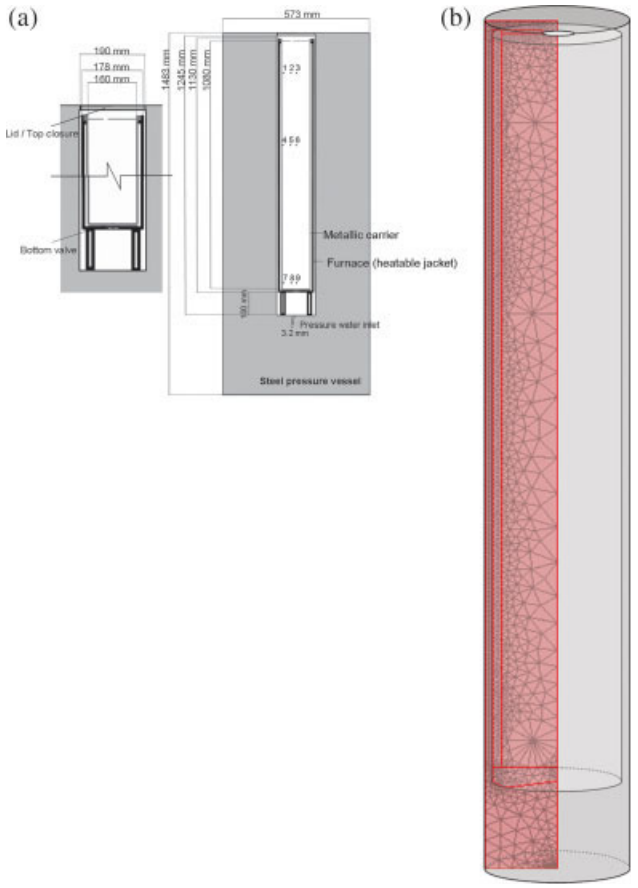

Figure 2. Vertical cross section of the high pressure vessel steel structure containing the furnace and carrier with their specified dimensions (a) and configuration of model geometry (b).

The outer cylinder shows the high pressure chamber, the inner cylinder the carrier, and the shaded area the computational domain due to axis-symmetry. [Color figure can be viewed in the online issue, which is available at www.interscience.wiley.com.]

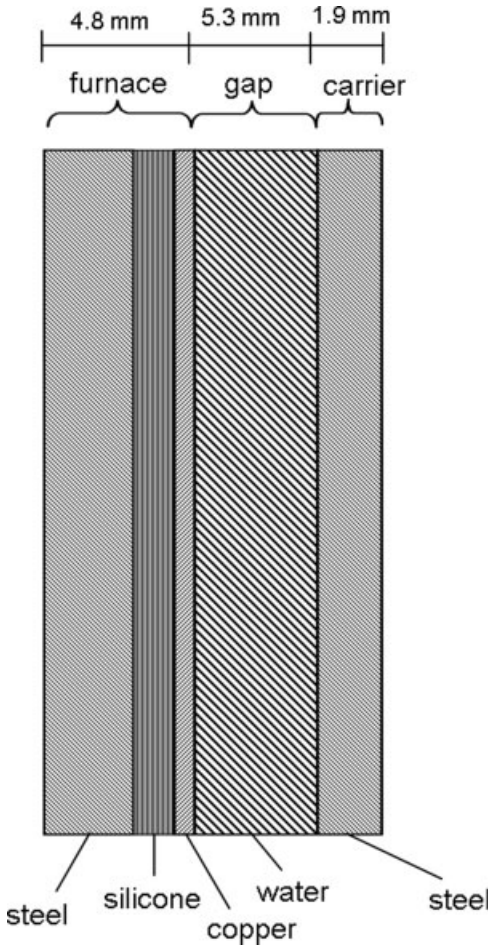

Figure 3. Composite structure of furnace and carrier (including water filled gap).

thick wire wound cylindrical stainless steel vessel (capacity 35 L) with two restrained end closures, an external low pressure pump, an intensifier, and necessary system controls and instrumentation.[10,36] The system closes automatically by a hydraulic system controlled by a PLC that inserts the lid at the top closure. Preheated water is injected from the bottom of the vessel through a 3.2 mm diameter pipe. The intensifier uses preheated water from the low pressure pump to generate high pressure fluid for compression. The high pressure vessel is designed with stainless steel food contacting parts so that potable water can be used as the isostatic compression fluid.[10] The stainless steel vessel is heated by resistors surrounding the structure (maximum temperature 90°C). Water can also be circulated through the vessel to ensure thermal equilibrium before pressurization.

Different inserts for preheating and carrying food were designed by Avure Technologies to be placed in the pressure vessel:

(i) An internal metallic cylinder composed by a multilayered structure (stainless steel/silicone/copper/water/stainless steel, Figure 3) with a brass base and a valve at the bottom. This metal composite carrier is located inside the chamber at less than 6 mm from the vessel wall.

(ii) A PTFE carrier centered in the same position as the metallic composite cylinder, with an internal diameter of 114 mm and an internal depth of 955 mm. The carrier walls are 26 mm thick at the walls and 20 mm thick at the bottom. This distance between the external carrier walls and the internal steel vessel walls is 12 mm.

Both carriers contain valves at the bottom that can be opened to inject hot water during preheating in a tank. After preheating the carrier reaches the initial chamber temperature and is transported into the vessel for pressurization.

Carrier (i) incorporates four thermocouples (k-type, Omega Engineering Inc.) to measure temperature at different points in the vessel. Temperature measurements were carried out inside the metal composite carrier at selected points 1 through 9 as shown in Figure 2a. Eight runs were carried out to measure temperatures in carrier (i). Before all trials, the four thermocouples were calibrated by placing them at the center of the carrier, and by placing the carrier in the preheating tank filled with water. Preheating measurements at 277, 333, and 368 K were compared to a PT-100 reference probe and correction factors determined for each thermocouple at ambient pressure. Nine temperature measurement positions were selected as shown in Figure 2a by fixing three of the thermocouples in plates belonging to an inner support rack. Top, middle, and bottom positions were at 39, 665, and 945 mm from the bottom inside the metal composite carrier, whereas each plate contained thermocouples located at a radial distance of 0, 30, and 65 mm from the central axis. The position of each of three thermocouples was rotated randomly in eight replicated runs and the fourth thermocouple stayed in position 6 as a "reference" run (resulting in two to eight replicates according to the position). Temperature was recorded every 5 s. Pressure runs were held at 600 MPa for 285 s. The temperature for the low pressure tank water, and pressure vessel walls was set to 363 K, while the final temperature was approximately 388 K.

Model

Geometry. The geometry of the model high pressure chamber is depicted in Figure 2b. The model has been designed to be a good approximation of the high pressure system described earlier. The real system incorporates some non-axis-symmetric features, notably the pressurizing fluid inlet; however, to make the problem more tractable, an axis-symmetric system has been simulated, with the fluid inlet moved to the centerline as shown.

The model consists of the chamber space, a water inlet at the bottom center, the carrier, and a water domain. Three scenarios were considered for thermal and fluid dynamic simulation:

(1) the chamber with no carrier
(2) the chamber including the metal composite carrier of (i) above (carrier volume 17 L)
(3) the chamber including a PTFE carrier of (ii) above (carrier volume 10 L)

In all scenarios, two modeling application modes, included in the modeling software and described later, were chosen and coupled: (i) the k-ε Turbulence model, applied to the water domain only (being inactive at the solid regions occupied by the carrier), and (ii) the Convection and Conduction model applied in both liquid and solid regions.

Governing Equations. The thermodynamic and fluid-dynamic behavior of the pressure medium is described by conservation equations of mass, momentum and energy.[27] Because of turbulent conditions, the equations for energy and momentum conservation have to be extended by further terms, which take the contributions of arising eddies (increased thermal conductivity due to mixing, increased dynamic viscosity due to increased shear) into account.

The development of a flow field during compression can be shown with the mass balance:

$$\frac{\partial \rho}{\partial t} + \nabla \cdot (\rho \vec{v}) = 0 \tag{6}$$

where $\vec{v}$ is the velocity vector. The relationship defines the density of water as a function of temperature and pressure and it is expressed as a simple polynomial $\rho = aP + bT + c$, which differentiated with respect to time gives:

$$\frac{\partial \rho}{\partial t} = a\frac{\partial P}{\partial t} + b\frac{\partial T}{\partial t} \tag{7}$$

Hence, density changes in time with pressure and temperature result in fluid motion.

Momentum conservation follows the Navier–Stokes equation.[37,38]

$$\rho\left[\frac{\partial \vec{v}}{\partial t} + (\vec{v} \cdot \nabla)\vec{v}\right] = -\nabla P + \nabla \cdot (\eta \cdot \nabla \vec{v}) + \rho g \tag{8}$$

where η represents the dynamic viscosity of the compressed fluid and g represents the gravity constant.

As shown later, the inflowing pressurization water enters through the high pressure system inlet at a high velocity and creates turbulent flow at the bottom region. To solve this flow, averaged representation is necessary by employing Reynolds Averaged Navier–Stokes (RANS) equations[39,40] comprising terms that include average velocity and pressure values and a fluctuating term (represented by the Reynolds stress tensor). In this case, a k-ε model was applied by including an additional "turbulence viscosity" to the equation for momentum conservation.[39,40] The k-ε closure scheme is one of the most used turbulence models for industrial applications.[40] The turbulent viscosity η_{T} is given by:

$$\eta_{\mathrm{T}} = \rho C_{\mu}\frac{k^2}{\varepsilon} \tag{9}$$

where C_{μ} is a constant, k is the turbulent kinetic energy, and ε the dissipation rate of turbulence. Here the momentum equation (extended according to COMSOL Multiphysics[40]) gives the following expression:

$$\rho\left[\frac{\partial \vec{v}_{\mathrm{a}}}{\partial t} + (\vec{v}_{\mathrm{a}} \cdot \nabla)\vec{v}_{\mathrm{a}}\right] = -\nabla P_{\mathrm{f}} + \nabla \cdot ((\eta + \eta_{\mathrm{T}}) \cdot \nabla \vec{v}_{\mathrm{a}}) + \rho g \tag{10}$$

where $\vec{v}_a$ denotes the average velocity and P_{f} includes a fluctuating term. In addition to the continuity equation, the k-ε closure includes two extra transport equations solved for both k and ε using model constants from experimental data.[40]

The k-ε closure equations were coupled with the energy conservation equation for heat transfer through convection and conduction, assuming nonisothermal flow. This equation was modified (from Kowalczyk et al.[37] and extended according to COMSOL Multiphysics[40]) by including the turbulent thermal conductivity k_{T}:

$$\frac{\partial(\rho C_P T)}{\partial t} + \nabla \cdot (\rho \vec{v} C_P T) = Q + \nabla \cdot ((k_1 + k_T)\nabla T) \tag{11}$$

where k_1 is the thermal conductivity, and C_p is the specific heat capacity. The source term Q arises from compression, by rewriting Eq. 3:

$$Q = T\alpha_{\mathrm{P}}\frac{dP}{dt} \tag{12}$$

Flow and heat transfer are thus coupled.

Process, Initial, and Boundary Conditions

Process conditions. The pressure-time profile is defined in the program as an input: it increases from ambient pressure to 600 MPa over 130 s, corresponding to a water compression, β, of 17%. On the basis of this, inlet velocity v_{in} was calculated using:

$$v_{\mathrm{in}} = \frac{\beta \cdot V_{\mathrm{water}}}{t_h} \cdot \frac{4}{\pi d^2} \tag{13}$$

where V_{water} is the volume of water inside the vessel (excluding carrier volume), t_{h} the pressure come up time, and d the diameter of the inlet tube (3.2 mm). The conditions defined above provide inlet velocities of 3.3, 4.8, and 5.7 m/s for the vessel with the PTFE carrier, the vessel with the metal composite carrier, and the vessel without carrier respectively. Inlet Reynolds numbers are between 36,000 and 60,000, so the plume of fluid entering the vessel is turbulent.

Once the maximum pressure is reached the inlet tube is closed and the pressure maintained for a set time (here 285 s). After the pressure holding period the inlet tube opens and water flows out according to a set pressure decrease from 600 MPa to atmospheric pressure over 15 s.

Initial conditions. The pressure chamber is completely filled with water at the start of the process. The pressure medium is initially at rest and the carrier, the vessel wall, and pressure medium are in thermal equilibrium at 363 K. So for $t = 0$, $T = T_0 = 363$ K $\forall r$, $\forall z$

Boundary conditions. These had to be defined for both applications modes as fluid-solid boundaries (for the k-ε Turbulence Model) and as thermal boundaries (for Convection and Conduction model). Preliminary work was carried out to determine appropriate simplifications of the problem. Given the axis-symmetric nature of the problem, boundary conditions for symmetry on the axis ($r = 0$) were assumed:

$$-k_1\frac{\partial T}{\partial r}\Big|_{r=0} = 0 \text{ and } -\eta\frac{\partial \vec{V}}{\partial r}\Big|_{r=0} = 0 \ \forall z, \quad \forall t > 0 \tag{14}$$

Fluid-solid boundaries. It was found necessary to define an inflow velocity boundary condition for the inlet tube for come up and holding times. Thus,

$$v_{\mathrm{z}}\big|_r = v_{\mathrm{in}} \quad \forall r, \quad 0 < r < 1.6 \text{ mm}, \ 0 < t < t_{\mathrm{h}}; \quad t_{\mathrm{h}} = 130 \text{ s} \tag{15}$$

$$v_{\mathrm{in}} = 0 \ \forall t, \quad t > t_{\mathrm{h}}$$

A pressure condition was also imposed in this boundary:

$$\frac{\partial P}{\partial t} = p_{\text{rate}} \quad \forall z, \forall r, \forall t > 0 \tag{16}$$

For come up time: $p_{\text{rate}} = P_{\text{target}}/t_{\text{h}} = 4.62$ MPA/s $\forall t$, $0 < t < t_{\text{h}}$
For holding time: $p_{\text{rate}} = 0$ and $P = P_{\text{target}} = 600$ MPA $\forall t$, $t_{\text{h}} < t < t_{\text{r}}$
where $t_{\text{r}} = 415$ s.

For decompression a normal flow pressure condition was imposed. In this case, the change in pressure was assigned to vary as follows:

$$p_{\text{rate}} = \frac{P_{\text{target}}}{t_{\text{f}} - t_{\text{r}}} = -40 \text{ MPa/s } \forall z, \forall r, \forall t, \quad t_{\text{r}} < t < t_{\text{f}} \tag{17}$$

where $t_{\text{f}} = 430$ s.

A logarithmic wall function condition is assumed at both the vessel and the carrier walls. The k-ε turbulent model allows accounting for turbulent transport in states close to isotropic. However, close to solid walls turbulence transport is no longer isotropic, as the fluctuations resulting in turbulence vary greatly in magnitude and direction. At these regions, deviations from isotropy are no longer negligible and must be accounted for in a proper model, like the law of the wall.

There are basically two approaches to account for solid walls subjected to turbulent flow. In the first approach, for low Reynolds number turbulent models, the equations are modified by additional terms and factors that account for near-wall effects. In such a case, the mesh must be refined near the wall so that the so-called viscous sublayer can be resolved. Such methods are of interest for moderate Reynolds numbers, where near-wall resolution leads to a reasonable number or elements.

In the second approach, chosen here, an empirical relation between the value of the velocity parallel to the wall and wall friction replaces the thin boundary layer near the wall. This empirical relation is the logarithmic wall function which expresses the wall velocity as a function of the friction velocity and length scale (which depend on the wall shear stress, the density of the fluid, and the viscosity). It also includes the constants characteristic of the wall surface. Part of the analysis of this condition includes identifying relevant scales for the turbulent kinetic energy k and the turbulence energy dissipation rate ε used in the k-ε turbulent model by considering the equilibrium boundary layer with a logarithmic profile. The logarithmic wall function model is accurate for high Reynolds numbers and situations where pressure variations along the wall are not very large. However, the method may be used outside its frame of validity with reasonable success.[40]

Thermal boundaries. Different approaches can be found to describe the inner steel chamber-fluid boundary. Most common, is the assumption of the inner wall temperature being constant in time and space.[32] Later approaches describe heat transfer into the wall on the basis of a one dimensional finite difference model.[29] Preliminary simulations were done to model the effect of increasing the bulk fluid temperature on the wall. A linear increase of the wall temperature during the pressurization step and a linear decrease during the pressure holding step were found. To minimize computational complexity, this wall temperature profile was programmed into the model. During the decompression step the temperatures at the walls were assumed constant. Thus:

$$T_{\text{wall}} = pt + q \quad \forall z, \forall r, \tag{18}$$

where

$$p > 0 \quad \forall t, \quad 0 < t < t_{\text{h}}$$
$$p < 0 \quad \forall t, \quad t_{\text{h}} < t < t_{\text{r}}$$
$$p = 0 \quad \forall t, \quad t_{\text{r}} < t < t_{\text{f}}$$

This assumption was based on results (not shown) from a separate 2D heat transfer simulation, where steel walls (drawn according to the HP vessel dimension) were located at the water boundaries where continuity was assumed. The top wall was assumed to provide thermal insulation.

$$-k_1 \frac{\partial T}{\partial z}\Big|_{z=L} = 0 \ \forall r, \forall t > 0 \tag{19}$$

where L is the inner vessel height.

The inlet boundary had a constant temperature condition until the end of the holding time, i.e.: $T_{in} = 358$ *K*, $\forall t$, $0 < t < t_r$, $0 < r < 1.6$ mm, $z = 0$. Another boundary condition to be considered is the continuity of heat flux at the carrier walls, $-k_1 \cdot \frac{\partial T}{\partial r} = k_{carrier} \cdot \frac{\partial T}{\partial r}, \forall r, \forall z \in$ specific boundary, $\forall t > 0$.

Material Properties. The physical properties, expansion coefficient, density, specific heat capacity, thermal conductivity, and viscosity of the pressurizing fluid water and their variation with pressure and temperature were obtained from NIST/ASME data base.[41] The software uses formulations for water properties developed and maintained by the International Association for the Properties of Water and Steam (IAPWS), as described in the software manual. The carrier material properties for steel, copper, silicone, brass, and PTFE were taken from the material database already integrated in the modeling software and is summarized in Table 2.

The data obtained in the relevant pressure and temperature intervals were then fitted by a first order polynomial in regards to both pressure and temperature: equations are given in Table 1. These equations were then implemented in the modeling software. Expansion coefficient within the solid materials (i.e., steel, PTFE, etc.) was assumed to be zero. Viscosity only had to be set within the water domains, active in the k-ε Turbulence Model.

Considering that the metal composite carrier is ~5 mm thick, and thereby very small finite elements would be required, composite physical properties were used for the

Table 1. Physical Properties of Water.

Property Y	a	b ($\times 10^6$)	c
C_{P} (J/kgK)	-0.1177	-0.6393	0.4134×10^4
k (W/mK)	0.1294×10^{-2}	0.3671×10^{-3}	0.2209
α (l/K)	0.1754×10^{-5}	-0.3513×10^{-6}	-0.6665×10^{-5}
ρ (kg/m^3)	-0.5597	0.2679	0.11839×10^4
η (Pas)	-0.3634×10^{-5}	0.2175	0.1645×10^{-2}

Property in the form of $Y = aP + bT + c$ where Y is the property, P is the pressure in MPa, T is the temperature in *K*.

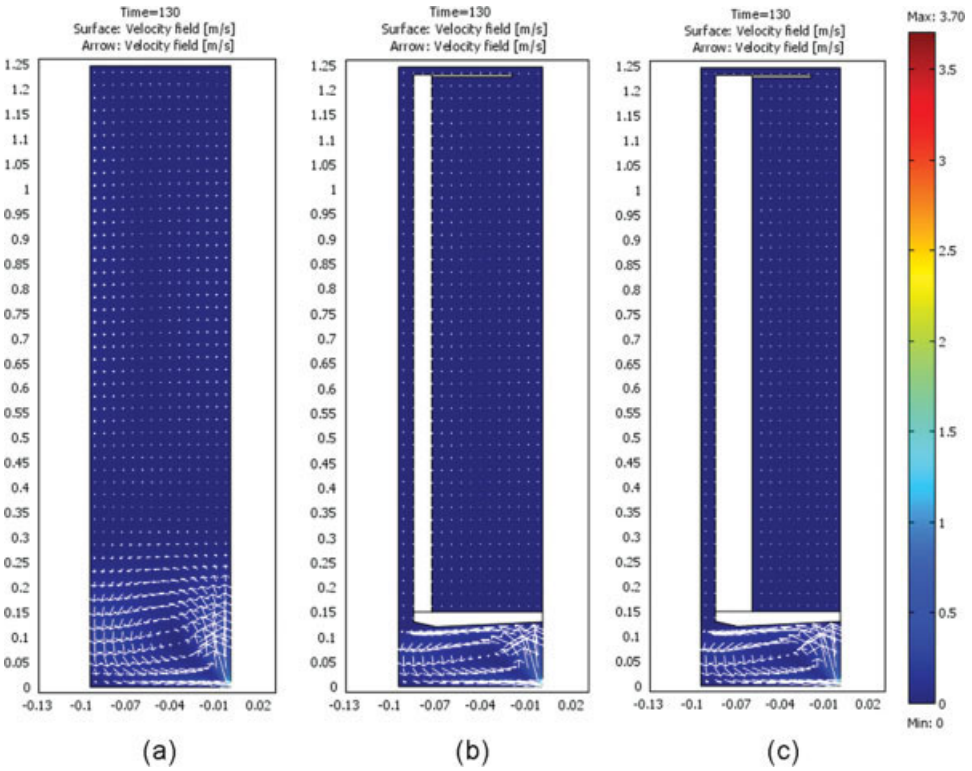

Figure 4. Velocity field in (a) the empty pressure vessel, (b) the pressure vessel containing the metal composite carrier, and (c) the pressure vessel containing the PTFE carrier.

[Color figure can be viewed in the online issue, which is available at www.interscience.wiley.com.]

space occupied by the thin layers of the composite materials (including the gap filled with water as in Figure 3). These layers were combined to one sub-domain and material properties (density, specific heat capacity, and thermal conductivity) calculated according to Eq. 20

$$\rho_{\text{combined}} = \frac{\sum_{i=1}^{n} \rho_i \cdot l_i^3}{l_{\text{combined}}^3}; \quad C_{\text{p,combined}} = \frac{\sum_{i=1}^{n} C_{\text{p},i} \cdot l_i^3}{l_{\text{combined}}^3};$$
$$k_{1\ \text{combined}} = l_{\text{combined}} \left(\sum_{i=1}^{n} \frac{l_i}{k_{1i}} \right)^{-1} \quad (20)$$

With density ρ, specific heat capacity C_P, thermal conductivity k_1, layer thickness l and indices *combined* for the composite material and i for the different layers.

Computational Methods. The partial differential equations describing the model were solved with the finite element method (FEM). A commercial software package, COMSOL Multiphysics™ (COMSOL AB, Stockholm, Sweden) was used, incorporating toolboxes for simultaneously solving multi physic problems. Calculating the microorganism inactivation extent according to Eq. 1 was performed using a self-developed code in MATLAB 7.4™ (Mathworks, Natick, MA).

The computations were carried out on a workstation running the 64bit OS Windows 2003 server. Two dual-core processors (CPU speed each 2.33 GHz) and a RAM of 4 GB allowed to solve the problem within 1 h of computation time. No significant differences in velocities and temperatures were found when the number of elements in the model was quadrupled.

Model Validation. Temperature validation was performed by comparing average temperature profiles at measured points (Figure 2a) with profiles provided by the model at the same locations. A MATLAB routine was developed to plot averaged real temperature profiles including confidence intervals at specific points in time and simulated profiles. The routine is also able to perform linear regression between measured and validated data at 14 points in time and to calculate how many points lie outside the confidence intervals.

Calculation of the Inactivation Distribution Inside the Vessel. A MATLAB routine was developed to extract temperature data from the model in COMSOL and transform it into 2D matrices containing vectors representing temperatures in time for each point of the vessel. These vectors were transformed into a single F value using Eq. 1 for each point of the vessel ($T_{\text{ref}} = 121.1^{\circ}\text{C}$ and $z_{\text{T}} = 10^{\circ}\text{C}$ for *C. botulinum*). The second part of Eq. 1 was also used to determine the reduction from each individual F value and obtain a plot of the distribution inside the vessel.

Simulation Results and Discussion

Vessel without carrier

Simulations are first presented for the empty pressure vessel, and are shown in Figures 4a and 5. Figure 4a shows the flow field in the vessel after 130 s, during pressurization. The

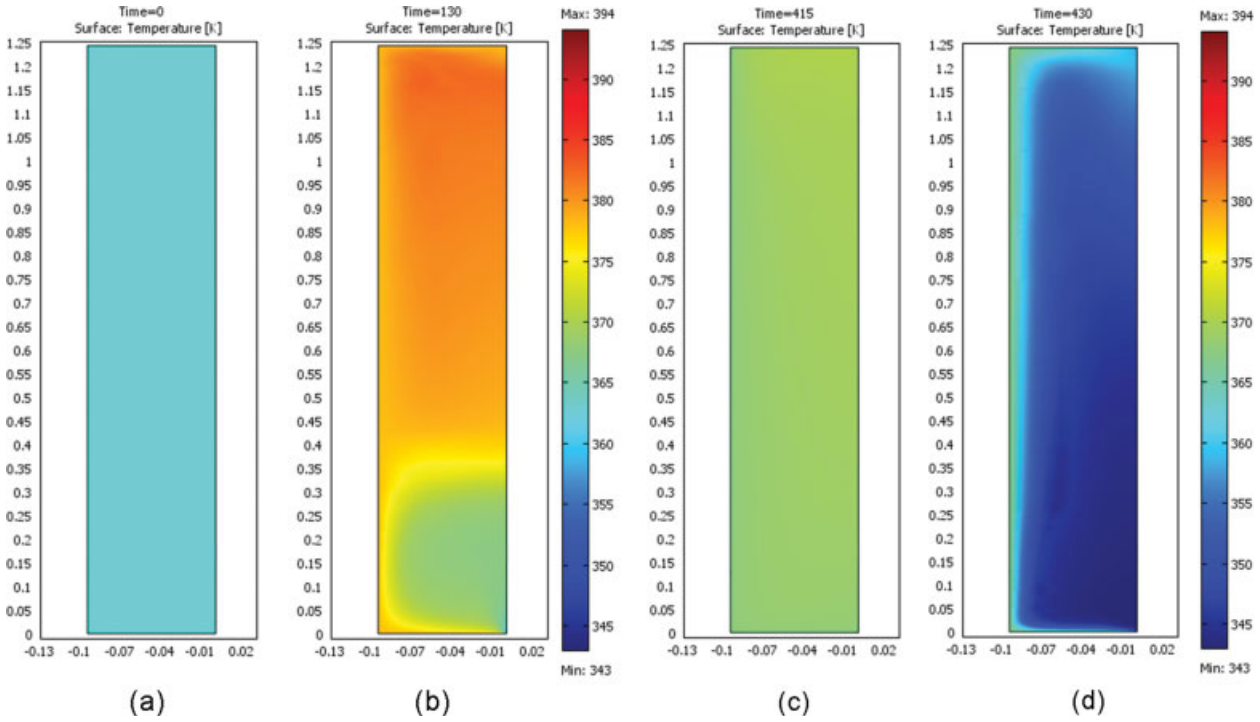

Figure 5. Thermal and flow profiles in the vessel without carrier.

Temperature distributions at (a) 0 s, (b) 130 s (end of come up time), (c) 415 s (end of holding time), and (d) 430 s (come down time). [Color figure can be viewed in the online issue, which is available at www.interscience.wiley.com.]

use of the stochastic k-ε turbulence model allowed identification of both laminar and turbulent regions inside the vessel. A plume of turbulent fluid enters the vessel forming a circulation region at the base, with high velocities (>1.5 m/s) are seen at the inlet. In the rest of the vessel flows are significantly lower, with laminar velocities (Re < 2000) decreasing towards the top. When modeling an empty vessel, other authors also observed flow deceleration from the inlet when water was incoming at 0.001–0.01 m/s.[30,34]

The flow is driven by the density change on pressurization. Natural convection as a result of temperature changes (Eq. 7) has a minor effect on flow during pressure application. A major horizontal shock wave was seen to propagate from bottom to top at about 10 s of pressurization, then reaching a quasi-constant flow pattern until the end of the come up time. Once pressurization is stopped and pressure held, the plume disappears within 8 s leaving laminar flow throughout the vessel. At this point flow is predominantly driven by gravitational (buoyancy) forces which need to be included in the model to provide a realistic flow pattern.

Hartmann and Delgado[26] observed transient flow during pressure come up and holding at 500 MPa and room temperature. However, in our models we observed a constant dynamic flow immediately after the shockwave propagation. During decompression, a vertical shockwave propagates from side to side breaking the laminar flow distribution (peak Re 2100) at the end of the 15 s decompression period.

Temperature profiles are shown in Figures 5a–d, corresponding to the start and end of the come-up time, the end of the holding period, and the end of the depressurization time. The images clearly show the problems that result from the absence of any method of retarding heat transfer from the fluid to the vessel walls:

- Figure 5a verifies the constant temperature (363 K) imposed at time zero.
- At the end of the pressurization stage (Figure 5b) the top 2/3 of the vessel has reached 378 K (maximum temperature 383 K). The cooling effect of the inlet flow is clear, appearing as a region of low temperature; the wall regions are also colder than the bulk because of conductive loss into the vessel.
- At the end of the 5 min holding stage, shown in Figure 5c the heat loss to the wall has continued, with bulk temperatures in the order of 369 K, less than 7 K above the starting temperature of 363 K. At this temperature sterilization reactions would be unacceptably slow.
- After depressurization the temperature distribution reversed, shown in Figure 5d; the bulk of the water in the vessel has a temperature of 345 K *below the starting condition*, a darker blue in the Figure. This appears strange; but arises because of the loss of heat into the stainless steel during the holding stage. The wall region is now warmest; eventually heat transfer from the pressure vessel will equilibrate the temperature at 363 K.

The simulations demonstrate the need to provide some thermal insulation to the system as well as some physical means to block the flow of the colder inflowing pressure media, which in this work was given by the carrier. The pressure vessel temperature is in practice limited both by the specified design tolerance of the steel material and the need

Table 2. Physical Properties of Vessel and Carrier Materials

Property	Steel	Copper	Water	Silicone	Composite*	Brass	PTFE
C_p(J/kgK)	475	385	4200	730	2234	390	1050
k(W/mK)	44.5	400	0.7	1.4	1.6	109	0.24
ρ(kg/m^3)	7850	8700	1000	2200	4358	8500	2200

*Calculated using Eq. 23.

to fill the batch vessel with water and product before pressurization. Thus, temperature must be less than 100°C; 90°C (363 K) is a compromise which minimizes bubble formation (i.e., limit internal vapor pressure in packages to prevent bulking during preheating and retain package integrity) while being hot enough to enable the system to reach sterilization conditions.

The simulations confirm the effect of scale found by Hartmann and Delgado.[42] They observed lower temperatures at the inlet region due to the forced convection of inflowing cold liquid in vessels of 6.3 and 50.3 L. However, Hartmann and Delgado[42] and Otero et al.[33] did not observe any influence of the incoming fluid when modeling small vessels of 0.8 and 0.75 L, respectively. Small vessels will have a higher surface to volume ratio and thereby proportionally faster cooling through the walls. However, lower temperatures near the inlet even for a 0.3 L vessel were determined by the model from Ghani and Farid.[34]

Vessel including the metal composite carrier

In this scenario the metal composite carrier (Figure 2) is used. The thermal properties of the carrier are shown in Table 2. There is a narrow channel (~6 mm wide) between the outside of the carrier and the pressure vessel wall.

Results of the simulation are given in Figure 4b for flow and Figure 6 for temperature distribution. The flow field shows that the turbulent plume now occupies the space underneath the carrier, and that flows elsewhere are significantly less. Fluid flows up the channel between carrier and wall and then enters the carrier. Velocities at the channel and inside the carrier are in the same order of magnitude as those found in the upper part of the empty vessel. A slight vertical flow channel develops inside the carrier as produced by the momentum transfer from the pressurization, with a peak of 0.06 m/s (Re = 640) against the wall and at the vessel center.

During pressurization, compression heating is only noticed above the carrier base, while the area underneath the carrier is 363 K for 10 s and gradually cools down to 358 K. At the end of pressurization, the temperature field is shown in Figure 6b; inside the carrier the temperature is significantly more uniform (~390 K in most part) than for the vessel without carrier, but there is still a cooler region above the base. Heat transfer from the carrier lower area to the brass base (and eventually to the water underneath the carrier) is noticeable at 40 s of pressurization. During the holding period the temperature equilibrates

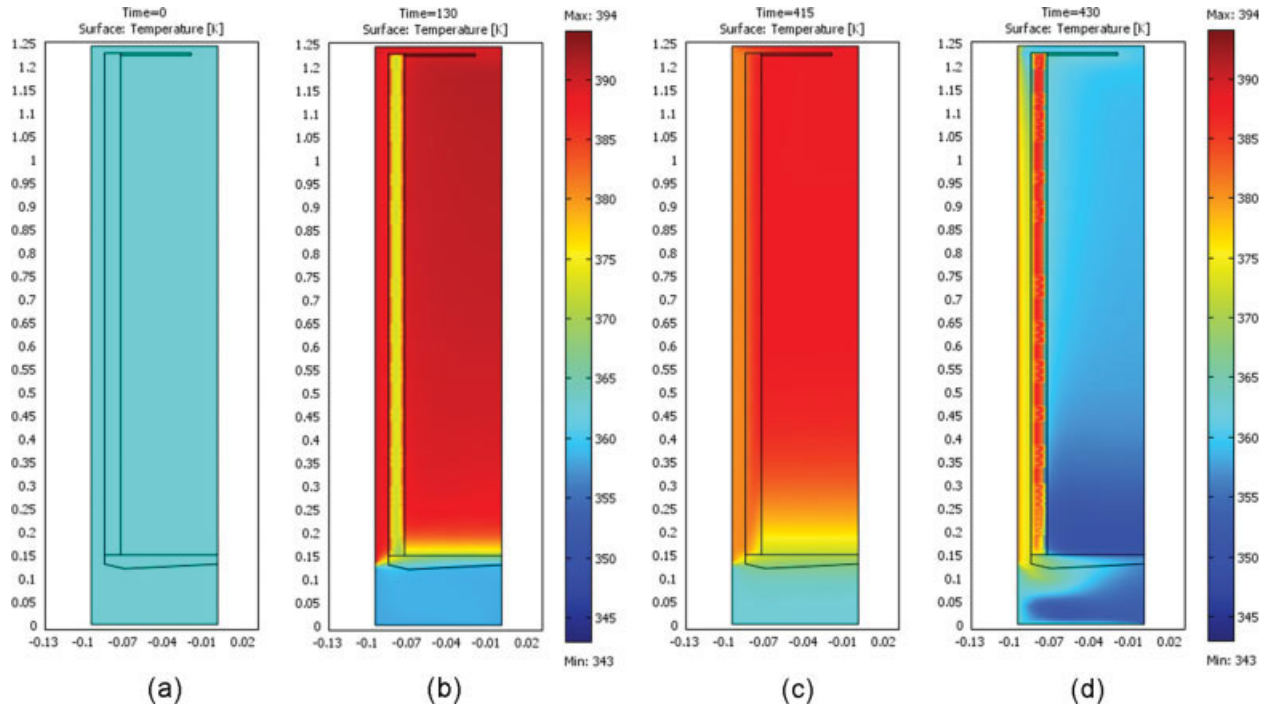

Figure 6. Thermal and flow profiles in the vessel containing the metal composite carrier.

Temperature distributions at (a) 0 s, (b) 130 s (end of come up time), (c) 415 s (end of holding time), and (d) 430 s (come down time). [Color figure can be viewed in the online issue, which is available at www.interscience.wiley.com.]

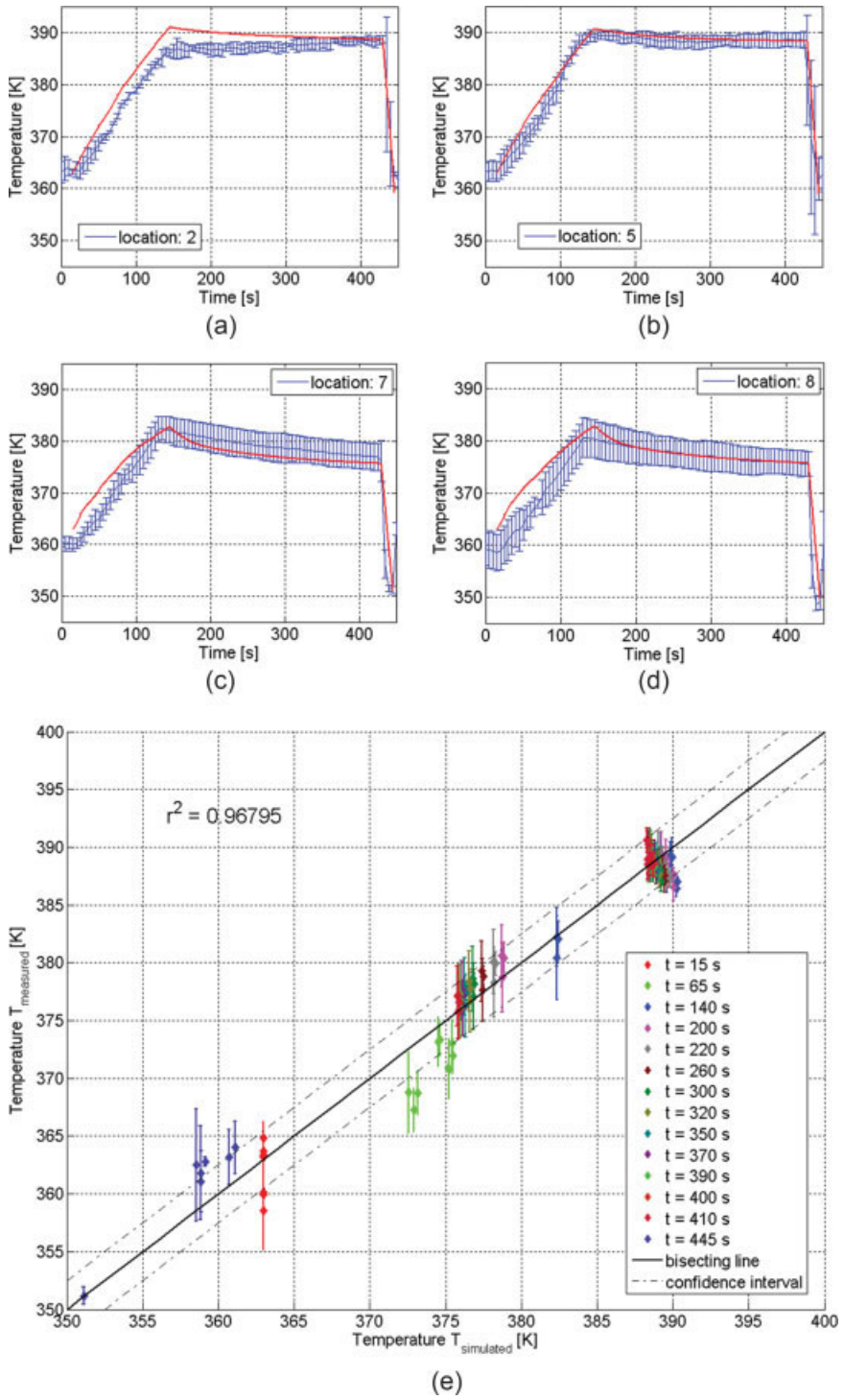

Figure 7. Model validation: (a), (b), (c), and (d) show the measured average temperature profiles (solid line with standard deviations) at locations 2, 5, 7, and 8, respectively, and the profiles predicted by the model (solid line not including standard deviations); the correlation between temperature values at all 9 thermocouple locations and predicted values are shown in (e).

[Color figure can be viewed in the online issue, which is available at www.interscience.wiley.com.]

inside the carrier, with the carrier rising in temperature (up to 388 K against the wall), while the fluid bulk cools from bottom to top (minimum 371 K and maximum 388 K). After depressurization the carrier is hottest while the fluid in the bulk of the vessel cools down to below the original 359 K at the top and centre, while even being below this (~350 K) at the base of the

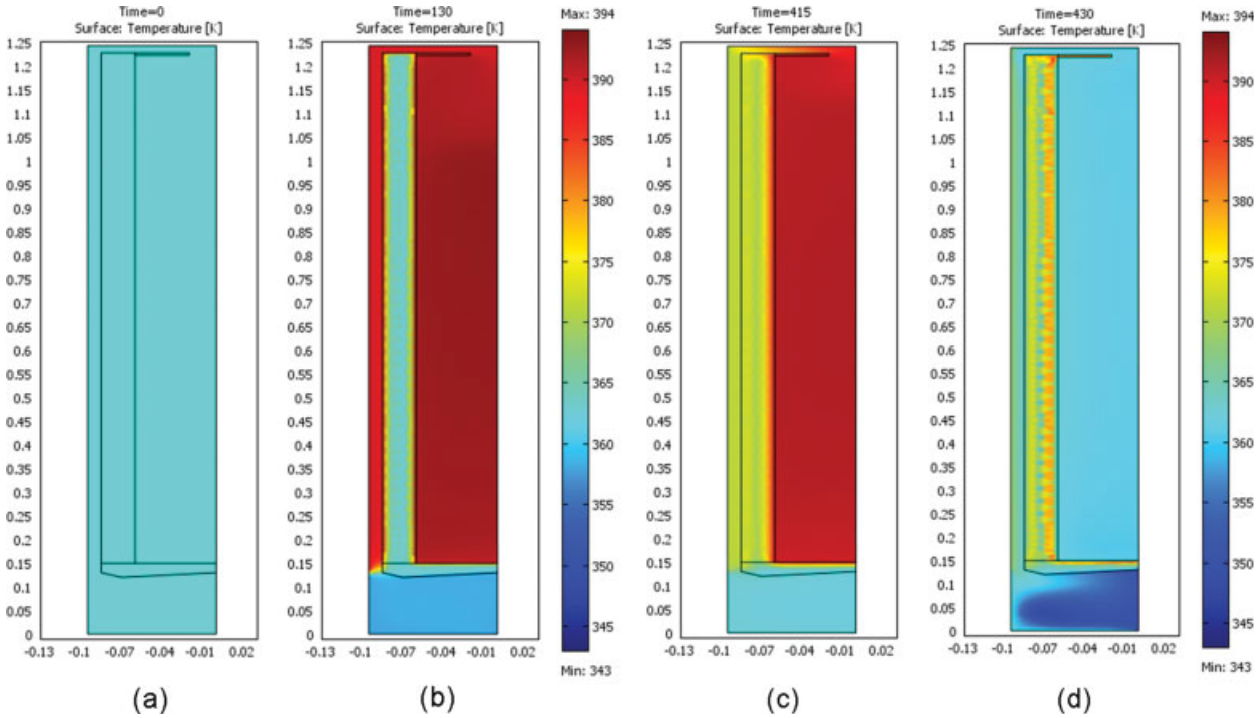

Figure 8. Thermal and flow profiles in the vessel containing the PTFE carrier.

Temperature distributions at (a) 0 s, (b) 130 s (end of come up time), (c) 415 s (end of holding time), and (d) 430 s (come down time). [Color figure can be viewed in the online issue, which is available at www.interscience.wiley.com.]

vessel. The temperature variation is less than that seen in the case without the carrier.

Figure 7 shows experimentally measured and predicted temperatures for four points within the carrier; one at the top of the carrier, one in the centre and two near the base region. The experimental data are well predicted, with the largest discrepancy being at the top of the carrier, where the model over-predicts temperature by 2 K. Confidence intervals of ± 2.5 K are based on the uncertainty of the positioning of the thermocouple (± 1 mm) and temporal resolution of the thermocouple (2 s). The overall match between experiment and model is given in Figure 7e; the plot shows lines at ± 2.5 K in which 92% of the data lie. As expected, the greatest difference between model and experiment arises at the start and end of the process where the changes in temperature are greatest. Overall the match between experimental data and the model is excellent ($R^2 > 0.96$).

Vessel including the PTFE carrier

The results of the previous sub-section showed that the presence of a carrier slowed down thermal conduction and momentum transfer in the vessel bulk, which led to greater uniformity in the temperatures within it. However, there was still a 17 K variation vertically in the composite carrier, giving a big difference in the rate of sterilization, as shown in the next section. Simulations have thus been conducted to investigate the effectiveness of using a carrier made from PTFE, 20 mm thick at the base and 26 mm thick at the sides, with a thermal conductivity of 0.24 W/mK and a thermal diffusivity of 1.6×10^{-7} m^2/s.

The simulation results are shown in Figure 4c; flow fields were essentially similar to those shown in Figure 4b. At the end of pressurization it can be seen that the low thermal conductivity of the PTFE has led to uniform temperature inside the carrier (392.5 K), with minimal heating of the PTFE. The cool regions are the entrance region caused by the plume (still around 358 K), the vessel-carrier channel, and the top part outside the carrier. The effect of thermal conduction during the holding stage is shown in Figure 8c in which (i) the temperature in the carrier is still uniform (391.5 K at the bulk region) with a variation of 1.5 K (ii) the temperature of the PTFE has increased slightly to 370 K. This time, the coolest region is at the top of the carrier (388.5 K), as a result of the cool down from the vessel-carrier channel fluid, and near the bottom (390.5 K). On the basis of calculations from Table 2, it is clear that the high thermal diffusivity of the brass base of the metal composite carrier allowed greater heat removal than the PTFE carrier, of much lower thermal diffusivity. After depressurization, the interior of the carrier is at about 363 K; the temperature pattern inside the PTFE is complex, with warm regions near the two edges, which result from heating during the holding period and a cold 'stripe' in the middle.

Temperature and sterilization profiles

Figure 9 plots the simulated temperatures at four of the points where thermocouples were placed in the validation

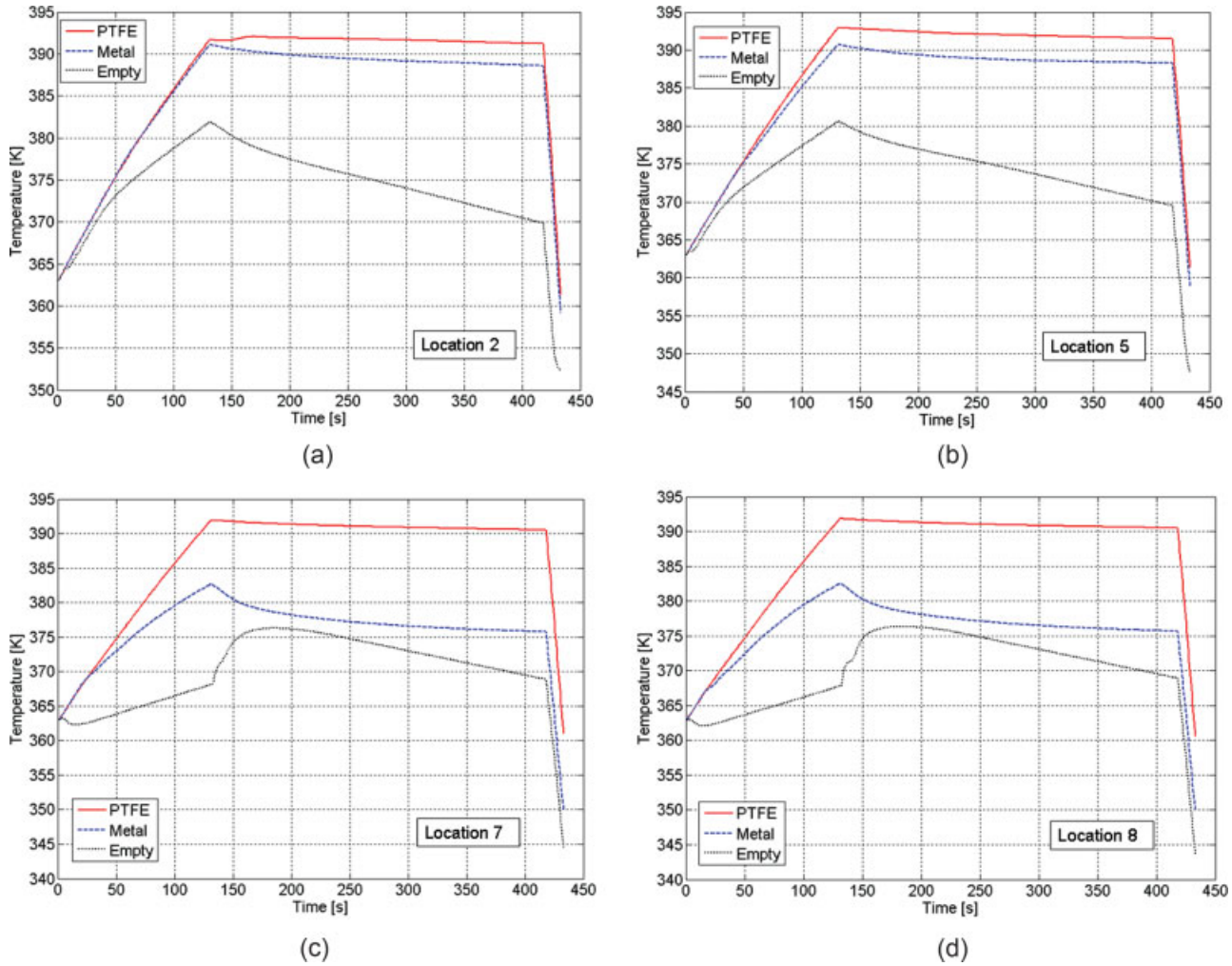

Figure 9. Predicted temperature profiles in all simulated scenarios (empty vessel, vessel with metal composite carrier, vessel with PTFE carrier) in selected locations: (a) location 2, (b) location 5, (c) location 7, and (d) location 8.

[Color figure can be viewed in the online issue, which is available at www.interscience.wiley.com.]

experiments (points 2, 5, 7, and 8 in Figure 2) for the three cases above, showing:

- That the temperature differences in the first two cases are large, with a drop of >10 K during holding in the case without the carrier, and 2–6 K for the metal composite carrier depending on the thermocouple position. The lower two locations for the vessel without carrier show the effect of the plume, with rapid heating after the pressurization stage, when the plume stops.
- The axial difference in temperature is significant, with about 12 K difference for the metal composite carrier; the vessel without carrier is well mixed thermally with ~1 K difference.
- However, the PTFE system has a relatively uniform temperature profile, with a drop of 2 K during the holding period and a difference of about 1 K between the four temperatures.

The simulations demonstrate that the presence of a carrier is required in a vessel with wall temperatures held at 363 K or lower to give the necessary thermal conditions for sterilization—the uniformity of the temperatures is greater in the PTFE case which implies that the process will produce a higher quality product as the amount of over-processing required to cope with the non uniformity will be small.

Figure 10 shows the distributions of the fractions of spores killed during the process for the three cases (expressed as a number of factors of 10 reduction). It can be seen that:

- For the vessel without carrier there is less than an order of magnitude reduction in the level of spores, as a result of the cooling of the vessel and the resulting low bulk temperature.
- For the metal composite carrier the maximum cook is a little less than 9 log reductions, but the base region has much less inactivation, again in the order of 1 log. This variation is not acceptable in a commercial process; more uniform temperature is needed.
- For the PTFE carrier; however, over 94.6% of the length of the carrier shows 12 or more log reductions in spores (up to 14); the effect of thermal uniformity is reflected in a uniform kill level. This implies that even without controlling the inflowing pressurization fluid temperature almost the whole volume of the carrier can be used for product.

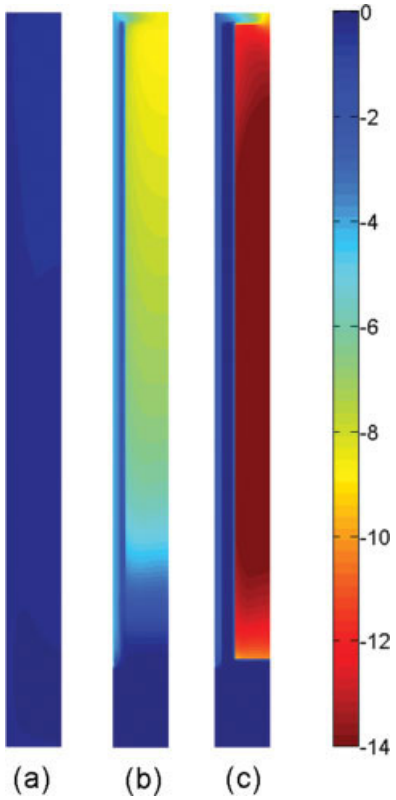

Figure 10. Predicted distribution of the extent of microbial log reduction in all simulated scenarios: (a) vessel without carrier; (b) vessel with metal composite carrier; and (c) vessel with PTFE carrier.

[Color figure can be viewed in the online issue, which is available at www.interscience.wiley.com.]

Discussion: implications for process design

The good agreement between the experimental data and the simulation shows the validity of the model, which can accurately predict the temperature changes that occur as a result of pressurization in an empty vessel or in a vessel with carriers of varied composition. No previous model includes a carrier inside the pressure vessel at HPHT sterilization and turbulent flow conditions. The flow pattern and temperatures are complicated, with a turbulent plume in the inlet region turning into a laminar flow between carrier and wall. To maximize the volume of food materials that can be processed per batch, there is a need to achieve uniform temperatures in regions as large as possible inside the pressure vessel.

In this case, the redesign of the carrier to substitute the metal composite carrier for a PTFE one has successful. It produces a very uniform temperature distribution (with temperatures in the region of 115–120°C, where sterilization is rapid) which is reflected in the uniformity of the F-value distribution inside the carrier. Temperature uniformity is not enough; the vessel without a carrier has a uniform temperature, but at too low a temperature. The calculation of the spore reduction extent considered only the temperature component. This conservative approach neglects a possible effect of pressure as an additional hurdle for inactivation.

Some factor will have to be added to provide a safety margin, and further validation experiments will be needed to provide evidence that the PTFE carrier is as successful as the model predicts. The model can be used both to optimize equipment design and process duration. For example, the carrier capacity could be increased, without endangering sterility, by reducing the thickness of the PTFE carrier, which seems to be too large as heat does not reach the centre of the carrier wall during the holding stage. Furthermore, if the furnace (or heatable jacket, Figure 2) is removed and the gap between carrier and wall is reduced the process could be used to generate at least 20 L/batch of sterile product, by removing the space taken [note that the actual inner volume is 10 L]. Other modifications include increasing the temperature of the inlet fluid and reducing the size of the hole at the top of the carrier to assure no cooling down at the top.

The simulations assume that no heating occurs in the pressurization of solid materials of making the carrier. This is an approximation of the real case, but a conservative one, as the solids may provide compression heating and thus provide greater insulation to the contained food. The effect of food packages on the process also needs to be established. The thermal properties of most foods, except lipids, are fairly close to that of water, but there is little data available on thermal properties (namely, specific heat, thermal expansion coefficient, and density) as a function of temperature and pressure, which allow predicting the ability of the packs to self-generate heat during compression. Assuming that packages heat by thermal conduction alone will be a highly conservative estimate, which will result in a low-quality product. It is of course possible that packages could overheat the carrier fluid, if for example the product's composition is increased in fat content, this case would be the best possible because it implies that the temperatures measured during the process are underestimates of those of the food and thus the products will be even more safe.

The model suggests that it will be possible to have thermal uniformity within the carrier, such that the losses through thermal conduction could be essentially neglected; under those conditions data such as shown in Figure 1 could be used as a design tool to suggest appropriate combinations of pressure and temperature.

Conclusions

In HPHT processing food is sterilized using the heat generated by pressurization. A model has been developed that accurately predicts temperature profiles during a sterilization process in a pilot scale (35 L) vessel; the model simulates both the fluid flow and convective and conductive heat transfer. Good agreement between the model and temperatures measured in a series of eight experimental runs was obtained. Significant cooling occurred when the vessel was empty while more uniformity was achieved when a carrier was inserted, acting as a barrier for flow and heat transfer. A PTFE carrier has been shown to provide a large region in the vessel in which there is uniform heating at all steps of the process. The inside of the PTFE carrier showed a uniform level of sterilization resulting from heating; the other cases gave unacceptable variations in sterility. Models of this type could be used both to design processes and equipment and to

demonstrate the safety of the process for industry and regulatory bodies.

Acknowledgments

PJF wishes to acknowledge financial support from a CSIRO McMasters Fellowship. Avure Technologies provided critical technical data and assistance during the project. The Victorian government is thanked for the Science and Technology Infrastructure grant which enabled the work to be carried out. Peerasak Sanguansri and Prof. Gustavo Barbosa-Cánovas are thanked for their contribution to experimental design.

Notation

a = constant (kg/m^3/MPa)
b = constant (kg/m^3/K)
C_p = isobaric heat capacity (J/kg/K)
$C_{p,combined}$ = composite specific heat (J/kg/K)
C_μ = constant (m^4/kg^4)
d = diameter of the inlet tube (m)
D = decimal reduction time (min)
F = thermal death time (min)
k = turbulent kinetic energy (kg^2/K^2)
k_1 = thermal conductivity (W/m/K)
$k_{1\ combined}$ = composite thermal conductivity (W/m/K)
g = gravity constant (9.8 m/s^2)
l = layer thickness (m)
L = inner vessel height (m)
N_0, N = initial and final number of microbial spores (cfu/L)
p = constant (K/s)
P = pressure (Pa)
P_f = pressure including a fluctuating term (Pa)
P_{target} = target pressure (600 MPa)
p_{rate} = pressure rate (MPa/s)
q = constant (K)
Q = volumetric compression heating rate (J/m^3/s)
T = temperature (K)
T_0 = initial temperature (363 K)
T_{ref} = reference temperature (121.1°C or 394.1 K)
t = time (s)
t_h, t_r, t_f = come up (130 s) release (415 s) and final pressurization times (430 s)
$\vec{v}$ = velocity vector (m/s)
$\vec{v}_a$ = average velocity vector (m/s)
$\vec{v}_{in}$ = inlet velocity (m/s)
r = radius (radial direction, m)
s = entropy (J/K)
V = specific volume (m^3/kg)
V_{water} = volume of water inside the vessel (excluding carrier volume, m^3)
z_T = thermal sensitivity (K)
z = vertical position (axial direction, m)

Greek letters

α_p = thermal expansion coefficient (1/K)
β = water compressibility (0.17)
ε = dissipation rate of turbulence energy (m^2/K^3)
η = dynamic viscosity (Pa·s)
η_T = turbulent viscosity (Pa·s)
ρ = density (kg/m^3)
$\rho_{combined}$ = composite density (kg/m^3)

Literature Cited

1. Norton I, Fryer P, Moore S. Product/process integration in food manufacture: engineering sustained health. *AIChE J*. 2006;52:1632–1640.
2. Holdsworth SD. *Thermal Processing of Packaged Foods*. New York: Blackie Academic and Professional, 1997.
3. Knoerzer K, Regier M, Schubert H. Microwave heating: a new approach of simulation and validation. *Chem Eng Technol*. 2006;29:796–801.
4. Marra F, Lyng J, Romano V, McKenna B. Radio-frequency heating of foodstuff: solution and validation of a mathematical model. *J Food Eng*. 2007;79:998–1006.
5. Zhang L, Fryer P. Food processing by electrical heating; the sensitivity of product sterility and quality to process parameters. *AIChE J*. 1994;40:888–898.
6. Hendrickx ME, Knorr D. *Ultra High Pressure Treatments of Foods*. New York: Kluwer, 2001.
7. Toepfl S, Heinz V, Knorr D. Overview of pulsed electric field processing for food. In: Sun DW, editor. *Emerging Technologies for Food Processing*, 1st edition. Elsevier Academic Press. 2005:69–97.
8. Matser AA, Krebbers B, van den Berg RW, Bartels PV. Advantages of high pressure sterilisation on quality of food products. *Trends Food Sci Technol*. 2004;15:79–85.
9. Margosch D. Behavior of bacterial endospores and toxins as safety determinants in low acid pressurized food PhD thesis, Technical University Berlin, Germany, 2005.
10. Farkas DF, Hoover DG. High pressure processing. In: Kinetics of microbial inactivation for alternative food processing technologies. Chicago, IL. *J Food Sci Suppl* 2000;65:47–64.
11. Margosch D, Ehrmann MA, Ganzle MG, Vogel RF. Comparison of pressure and heat resistance of *Clostridium botulinum* and other endospores in mashed carrots. *J Food Protect*. 2004;67:2530–2537.
12. Koutchma T, Guo B, Patazca E, Parisi B. High pressure-high temperature sterilization: From kinetic analysis to process verification. *J Food Process Eng*. 2005;28:610–629.
13. Ting E, Balasubramaniam VM, Raghubeer E. Determining thermal effects in high-pressure processing. *Food Technol*. 2002;56:31–35.
14. de Heij WBC, Van Schepdael LJMM, Moezelaar R, Hoogland H, Matser A, van den Berg RW. High-pressure sterilization: maximizing the benefits of adiabatic heating. *Food Technol (Chicago)*. 2003;57:37–41.
15. de Heij WBC, Van Schepdael LJMM, Moezelaar R, van den Berg RW. Sterilization by high hydrostatic pressure: Increasing efficiency and product quality by improved temperature control. In: *Advances in High Pressure Bioscience and Biotechnology,* Germany: Springer Verlag, 2003:367–370.
16. NC Hyperbaric. High Pressure Processing Equipment:WAVE 6000 RANGE. Available at: http://www.nchyperbaric.com/index.htm. Internet Communication. 13-7-2007.
17. Leadley C. High pressure sterilisation: a review. *Campden Chorleywood Food Res Assoc*. 2005;47:1–42.
18. Barbosa-Cánovas GV, Juliano P. Food sterilization by combining high pressure and heat. In: *Proceedings of the Iberoamerican Congress of Food Engineering* (*CIBIA V)*, Puerto Vallerta, Mexico 2007.
19. Krebbers B, Matser AM, Koets M, van den Berg RW. Quality and storage-stability of high-pressure preserved green beans. *J Food Eng*. 2002;54:27–33.
20. Juliano P, Clark S, Koutchma T, Ouattara M, Matthews JW, Dunne CP, Barbosa-Canovas, GV. Consumer and trained panel evaluation of high pressure thermally treated scrambled egg patties. *J Food Qual*. 2007;30:57–80.
21. Denys S, Ludikhuyze LR, Van Loey AM, Hendrickx ME. Modeling conductive heat transfer and process uniformity during batch high-pressure processing of foods. *Biotechnol Progr*. 2000;16:92–101.
22. Otero L, Sanz P. Modelling heat transfer in high pressure food processing: a review. *Innovat Food Sci Emerg Tech*. 2003;4:121–134.
23. de Heij WBC, Van Schepdael LJMM, van den Berg RW, Bartels PV. Increasing preservation efficiency and product quality through control of temperature distributions in high pressure applications. *High Pres Res*. 2002;22:653–657.
24. Ardia A, Knorr D, Heinz V. Adiabatic heat modelling for pressure build-up during high-pressure treatment in liquid-food processing. *Food Bioproducts Proces*. 2004;82(C1):89–95.
25. Denys S, van Loey AM, Hendrickx ME. A modeling approach for evaluating process uniformity during batch high hydrostatic pressure processing: combination of a numerical heat transfer model and enzyme inactivation kinetics. *Innovat Food Sci Emerg Tech*. 2000;1:5–19.
26. Hartmann C, Delgado A. Numerical simulation of convective and diffusive transport effects on a high-pressure-induced inactivation process. *Biotechnol Bioeng*. 2002;79:94–104.

27. Hartmann C, Delgado A, Szymczyk J. Convective and diffusive transport effects in a high pressure induced inactivation process of packed food. *J Food Eng*. 2003;59:33–44.
28. Carroll T, Chen P, Fletcher A. A method to characterise heat transfer during high-pressure processing. *J Food Eng*. 2003;60:131–135.
29. Hartmann C, Schuhholz J, Kitsubun P, Chapleau N, Bail A, Delgado A. Experimental and numerical analysis of the thermofluiddynamics in a high-pressure autoclave. *Innovat Food Sci Emerg Technol*. 2004;5:399–411.
30. Hartmann C. Numerical simulation of thermodynamic and fluiddynamic processes during the high pressure treatment of fluid food systems. *Innovat Food Sci Emerg Technol*. 2002;3:11–18.
31. Hartmann C, Delgado A. Behavior of bacterial endospores and toxins as safety determinants in low acid pressurized food. In: Hayashi R, editor. *Trends in High Pressure Bioscience and Biotechnology, Progress in Biotechnology*. 2002:533–540.
32. Hartmann C, Delgado A. The influence of transport phenomena during high-pressure processing of packed food on the uniformity of enzyme inactivation. *Biotechnol Bioeng*. 2003;82:725–735.
33. Otero L, Ramos AM, de Elvira C, Sanz PD. A model to design high-pressure processes towards an uniform temperature distribution. *J Food Eng*. 2007;78:1463–1470.
34. Ghani AGA, Farid MM. Numerical simulation of solid-liquid food mixture in a high pressure processing unit using computational fluid dynamics. *J Food Eng*. 2007;80:1031–1042.
35. Stumbo CR. *Thermobacteriology in food processing*. 2nd edition. New York: Academic Press, 1973.
36. Juliano P, Knoerzer K, Barbosa-Cánovas GV. Heat transfer modeling in low-acid food high pressure thermal sterilization processes. In: Simpson R, editor. *Engineering Aspects of Thermal Processing*. Boca Raton, FL: CRC Press. 2007.
37. Kowalczyk W, Hartmann C, Delgado A. Modelling and numerical simulation of convection driven high pressure induced phase changes. *Int J Heat Mass Trans*. 2004;47:1079–1089.
38. Chen XD. Modeling thermal processing using computational fluid dynamics (CFD). *Thermal Food Processing*, editor: Sun DW. Boca Raton, FL: Taylor & Francis. 2006:133–151.
39. Nicolaï BM, Verboven P, Scheerlinck N. Modeling and simulation of thermal processes. In: Richardson P, editor. *Thermal Technologies in Food Processing*. Boca Raton, FL: CRC Press, 2007:91–112.
40. COMSOL Multiphysics. In: *Chemical Engineering Module*. Stockholm, Sweden: COMSOL AB, 2006.
41. Harvey AH, Peskin AP, Sanford AK. NIST/ASTME—IAPSW Standard Reference Database 10, version 2.2. 1996.
42. Hartmann C, Delgado A. Numerical simulation of thermal and fluiddynamical transport effects on a high pressure induced inactivation. *High Pres Res*. 2003;23:67–70.

Manuscript received Jun. 1, 2007, and revision received July 13, 2007.